Journal of Power Sources 255 (2014) 1–8

Contents lists available at ScienceDirect

Journal of Power Sources

journal homepage: www.elsevier.com/locate/jpowsour

Long-term evaluation of solid oxide fuel cell candidate materials in a 3-cell generic short stack fixture, part I: Test fixture, sealing, and electrochemical performance

Yeong-Shyung Chou*, Jeffry W. Stevenson, Jung-Pyung Choi

K2-44, Energy and Efficiency Division, PNNL, Pacific Northwest National Laboratory, P.O. Box 999, Richland, WA 99354, USA

HIGHLIGHTS

- A generic stack fixture was successfully demonstrated in a 3-cell stack at 800 °C.
- Cell, seal system, interconnect plate, and electrodes were presented.
- Electrochemical performance of LSM-based cell over 6000 h was reported.
- LSM-based cell showed low degradation rate of 1–2% per 1000 h.
- Post-mortem analysis was conducted and cause of sealing failure was identified.

ARTICLE INFO

Article history:
Received 19 June 2013
Received in revised form
6 December 2013
Accepted 11 December 2013
Available online 24 December 2013

Keywords:
Sealing glass
AISI441
Aluminization
(Mn,Co)-spinel
SOFC

ABSTRACT

A generic solid oxide fuel cell stack test fixture was developed to evaluate candidate materials and processing under realistic conditions. A NiO–YSZ anode-supported YSZ electrolyte cell with a composite cathode was used to evaluate the long-term stability of a sealing system, alumina coating, Ce-modified (Mn,Co)-spinel coating, ferritic stainles steel AISI441 interconnect metal, and current collectors. A 3-cell short stack was assembled and tested in constant current mode for 6000 h at 800 °C. Part I of the work addresses the stack fixture design, cell components, sealing system, cell performance, and post-mortem analysis. Parts II and III will discuss microstructure evolution, interfacial reactions, and degradation mechanisms. During 6000 h of testing, the top cell showed very low degradation ($\sim$1.4% kh^{-1}), while the middle and bottom cells exhibited much higher degradation after $\sim$2000 h. The rapid cell degradation was correlated to the open circuit voltage measurements and was attributed to glass seal failure, probably due to unbalanced stress conditions. Post-mortem analysis showed a characteristic yellowish color around the glass seal, suggesting formation of $SrCrO_4$. Overall the developed stack test fixture was demonstrated as a simple and useful tool for evaluation of SOFC candidate materials in realistic conditions.

1. Introduction

Small sized button cells are widely used in solid oxide fuel cell (SOFC) research for materials processing, optimization, and characterization [1–5]. The small sized cells offer a fast turn-around in terms of fabrication and processing, as well as adequate mechanical strength for handling. On the other hand, the simplified button cells suffer from unrealistic gas flow patterns, sealing design, and current collectors. For example, in actual planar SOFC stacks, gases flow parallel to the cell surfaces, while they are perpendicular in button cells. As a result of direct impingement on electrodes, fuel and oxidant utilization and back pressure for button cells may differ considerably from actual stacks. Sealing is another major difference, not only in design and mating materials, but also in the choice of sealants. For button cells, sealing is generally applied directly to the circumferential edges of porous anode support edges, and the cell is typically sealed onto the end of an alumina tube. This combination of mating materials with large mismatch in coefficient of thermal expansion (CTE) often leads to poor thermal cycle stability with sealing glasses. Due to the porous nature of anode supports, no compressive mica seal can be applied to button cell tests with a porous anode support sealed onto alumina pipe. Also, metallic interconnects are not included in button cell test designs. As a result, the issues of Cr-poisoning [6–10] and oxidation or spallation of

* Corresponding author. Tel.: +1 509 3752527; fax: +1 509 3752186.
E-mail address: yeong-shyung.chou@pnnl.gov (Y.-S. Chou).

0378-7753/$ – see front matter © 2014 Published by Elsevier B.V.
http://dx.doi.org/10.1016/j.jpowsour.2013.12.067

metallic interconnects [11] cannot be investigated. In addition, precious metals such as gold or platinum mesh and/or contact paste are often used for current collectors. These materials cannot be used in commercial stacks due to cost issues. Finally, button cells operate isothermally (due to their small size) while there are significant temperature gradients within large cells and stacks. All of these facts tend to hinder technology transfer between button cells and real-size stacks. In a previous study on the effect of high water content fuel on cell performance, we have presented a simple test fixture for single cell test and candidate materials evaluation [12,13]. In this work, we will present a modified SOFC test fixture that allows for stack tests where multiple cells are assembled with internal manifolds for fuel and oxidant delivery. In addition, metallic interconnect plates with both anode and cathode features were included. A commercial Ni–YSZ anode-supported thin YSZ electrolyte cell (5 cm × 5 cm) with a lanthanum strontium manganite (LSM)–YSZ cathode (4 cm × 4 cm) was used as the baseline cell. Three candidate SOFC materials were investigated in the tests: a conductive protective coating consisting of Ce-modified (Mn,Co)-spinel on the cathode side of AISI441 interconnects, a refractory sealing glass for the cell-to-frame seal, and a protective coating of alumina at the sealing area. In Part I of this study, the stack test fixture, sealing systems, long-term electrochemical performance of each cell, and post-mortem analysis will be presented and discussed.

2. Experimental

2.1. Cell materials

Commercial NiO–YSZ anode-supported YSZ cells were used in this study (ASC-3 cell, H. C. Starck Ceramics, GmbH, Germany). The thickness of the porous anode support was about 500 μm and the thickness of the YSZ electrolyte was about 5 μm. The cell also had an active anode layer adjacent to the YSZ electrolyte layer of 5–10 μm thick. The porous cathode was composed of a thin (~10 μm) active layer of YSZ–LSM next to the electrolyte and a thicker (~30–50 μm) LSM porous cathode on top of the active cathode. The cell has an active cathode area of 16 cm^{-2} leaving a square circumferential band of 0.5 cm width for sealing onto the window frame plate. The details of the cell microstructure were given in Ref. [12].

2.2. Sealing materials and system

Two types of seals were used in the short stack tests. A high-temperature sealing glass (YSO77) was used for the cell-to-window frame seal, and a hybrid mica with glass interlayers for the perimeter seal. The glass (YSO77) was a Sr–Ca–Y–B–Si glass with a sealing temperature of ~950 °C, modified from the parent refractory sealing glass YSO1 [14]. The details of the sealing glass making, thermal property characterization, and glass powder processing are given in Ref. [14]. For the cell-to-window frame seal, the glass powders were mixed with an organic binder (ESL450, ElectroScience Lab, King of Prussia, PA) to form a paste, and applied onto the window frame plate. After drying, the cell-to-window frame was fired to 950 °C for 2 h followed by crystallization treatment at 800 °C for 4 h in air. After sealing, an iso-propanol penetration test was used to check the hermeticity by visual observation. The rigid and brittle nature of the sealing glass at room temperature would result in seal fracture if CTEs were not closely matched. The brittle fracture, if present, will always crack through the whole sealing width, which leads to quick penetration when using a low surface tension solvent like isopropanol. Only hermetic cells were used for short stack testing. In addition to the cell-to-window frame seal, a hybrid mica seal with glass interlayer was used as the perimeter seal (#2 to #7 in

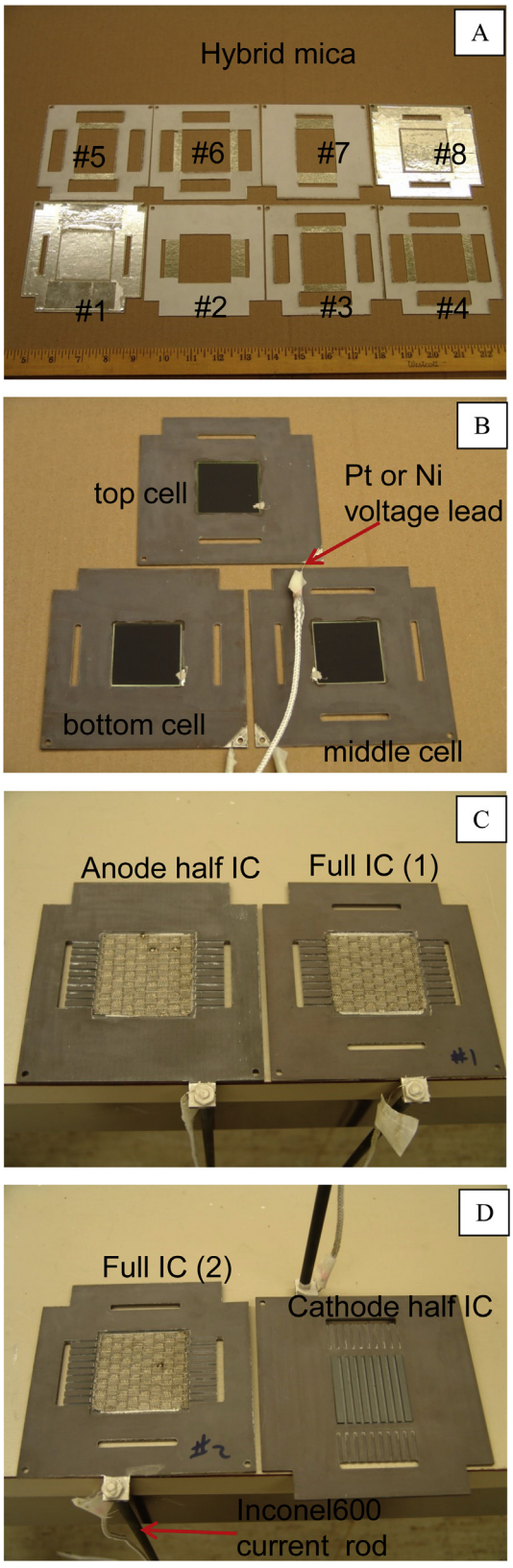

Fig. 1. Photographs showing the actual parts used for the 3-cell short stack test. (A) Eight hybrid mica seals with glass interlayers as well as Ag foil, (B) three sealed PEN/window frame plates, (C) two interconnect plates close to air heat exchanger, and (D) two interconnect plates close to fuel heat exchanger.

Fig. 1A) as well as hybrid mica with Ag interlayers for two heat-exchangers (#1 and #8 in Fig. 1A). The glass interlayers (about 250 μm thick) were prepared by a tape casting technique with a composite glass consisting of 25 wt% G18 (Ba–Ca–Al–B–Si) [15] and 75% YSO77 for better wetting between window frames and interconnect plates. Hybrid mica seals with Ag foil (25 μm) were used for sealing to the anode and cathode heat exchangers for easy cleaning and reuse purposes. The Ag hybrid mica was recently reported to offer excellent long-term stability and thermal cycle stability even under large CTE mismatch conditions [16,17].

2.3. Window frame, interconnect material and protective coatings

In this study, metallic window frames and interconnect plates were used for the short stack assembly. A ferritic stainless steel, AISI441 (ATI Allegheny Ludlum, Pittsburgh, PA), was selected as the candidate metal due to its good oxidation resistance, matching coefficient of thermal expansion with the anode-supported cell, the formation of a conductive oxide scale, and lower cost as compared to other candidate alloys such as Crofer22APU (ThyssenKrupp, Germany). AISI441 has a slightly lower Cr content (18%) than Crofer22APU and similar trace elements of Mn, Ti, Al, and Si [12]. It also contains Nb which can precipitate as a Laves phase, thereby capturing Si impurities along the grain boundaries. The capture of Si in the Laves phase minimizes the Si activity in the alloy matrix and prevents the formation of an insulating silica layer, resulting in a reduced area specific resistance (ASR) [18]. Two different thicknesses of AISI441 were used: 4.31 mm was used for the interconnect plates, and 1 mm was used for the window frame plate for cell sealing. Fig. 1B shows the three as-sealed cell to window frame plates with the black cathode facing up, and Pt lead wires welded for voltage measurements. The size of the window frame plate was about 120 mm × 120 mm with a central square hole of about 40 mm × 40 mm, and rectangular slots for gases. Three types of interconnect plates were made with the same nominal dimensions as the window frames: one facing the fuel heat exchanger, one facing the air heat exchanger, and two full interconnect plates in between, as shown in the stack assembly (Fig. 2). For full interconnect plates, there were four rectangular slots to provide for gas flow in a cross-flow pattern, while the plates facing heat exchangers only had two gas slots either for air or fuel to pass through, as shown in Fig. 1C and D. On the anode side of the interconnect plates, there were no straight machined grooves to guide the gas flow in the central section, while there were grooves on the cathode side of the interconnect plates (Fig. 1D). A corrugated Ni mesh was spot welded onto the interconnect plate on the anode side to serve as the current collector, as shown in Fig. 1C. Inconel 600 rods, used for current leads, were threaded onto the side tabs in the interconnect plates.

It is well known that Cr-containing steels cannot be directly used for SOFC applications, due to Cr volatility that can lead to cathode poisoning and chromate formation in sealing areas. Two protective coatings were used in this work: Ce-modified $Mn_{1.5}Co_{1.5}O_4$ spinel for the active cathode region, and aluminization for the remaining areas. $Mn_{1.5}Co_{1.5}O_4$ spinel was shown to provide good electrical conduction and to minimize the Cr-poisoning issues [6–10,18]. The $Mn_{1.5}Co_{1.5}O_4$ spinel coating also reduced the oxidation of the underlying metal substrate; however, the coating spalled off after an accelerated ageing test at 850 °C for 900 h [19]. The addition of a small amount of CeO_2 to $Mn_{1.5}Co_{1.5}O_4$ spinel showed some improvement in that no spallation was observed under the same accelerated oxidation test up to 1200 h, and therefore was adopted in this work. The details of the spinel coating including powder processing and the two-stage heat-treatment are given in Ref. [19]. The remaining areas of the

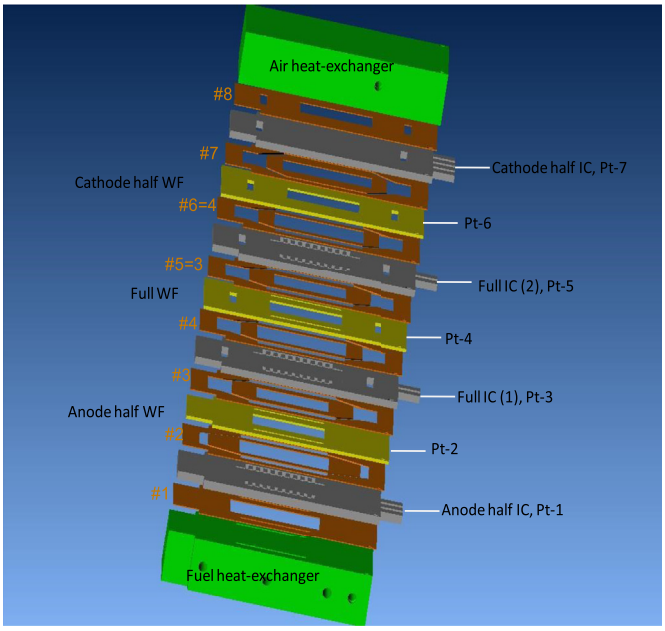

Fig. 2. Schematic drawing showing the assembly of the 3-cell short stack: three window frame plates in yellow, 4 interconnect plates in gray, 8 hybrid mica seals in brown. All were pressed between two heat exchangers for fuel and air, shown in green color. WF = window frame, IC = interconnect, Pt = platinum wire. (For interpretation of the references to color in this figure legend, the reader is referred to the web version of this article.)

interconnect plates and the entire window frames were aluminized using Al metal powder in a simple oxidation process. Without the alumina protection, sealing glasses containing alkaline earths (such as Ba and Sr) can spontaneously react with Cr in air and form undesirable chromates with very high CTEs [20,21]. As a result of large mismatch in CTE with mating SOFC components, fracture often occurs after sealing or repeated thermal cycling. The details of the aluminization process are given in Ref. [22]. The $Mn_{1.5}Co_{1.5}O_4$ spinel coating was about 5 μm thick with some residual porosity while the aluminized coating was 1–3 μm thick and dense. The details of the coating microstructure are given in Ref. [12].

2.4. 3-cell stack assembly, testing, and characterization

A schematic drawing of the 3-cell short stack assembly, including three window frame plates, four interconnect plates, and eight hybrid mica seals is shown in Fig. 2. The short stack assembly was compressed between two heat exchangers, one for incoming air and the other for the fuel; the gases were supplied in a cross-flow pattern. Inconel 600 superalloy was used to make the heat exchangers due to its high temperature creep and oxidation resistance. NiO powders (J.T. Baker, Phillipsburg, NJ) were used with binders to make a contact paste that was applied between the Ni-mesh and the cell's anode. At the cathode side, LSM-20 contact paste was applied between the (Mn,Co) spinel-coated interconnect plate and the cell's cathode. Seven Pt wires were spot-welded onto four interconnect plates and three window frames for voltage sensing. A compressive load of ~250 kPa was applied during the test. The stack was first dried at around 70 °C for several hours, then heated to 550 °C for binder burnoff. The stack was then heated at 3 °C min^{-1}–930 °C for 2 h for sealing and then cooled down to 800 °C for testing. Air was flowing in both the cathode and anode chambers before the cell was cooled down to 800 °C. The fuel side was then switched to a low hydrogen fuel (~5% H_2/bal. N_2) for several hours to reduce the NiO in the anode to Ni metal before

switching to slightly humidified fuel (H_2:N_2 = 1:1, H_2O ~ 3%) for testing. To confirm that there was no substantial leakage due, for example, to cell fracture, both the outgoing air and fuel lines were connected to a water bubblers with ~6 inches of water to provide an indicator of gas flow as well as to provide a small back pressure. The stack was tested at 800 °C in a constant current mode. The electrochemical performance (impedance and IV sweep) of each cell was measured with an electrochemical test unit (Model VSP and VMP3B, Bio-Logic SA, Princeton Applied Research, Oak Ridge, TN). After the test, the stack was dis-assembled and post-mortem analysis was conducted with optical microscopy. Areas of primary interest were sectioned and polished for interfacial and microstructure analysis; those results will be presented in the second and third part of this work.

3. Results and discussion

3.1. Generic stack design

A planar stack design was chosen in this work for developing a generic test fixture to validate SOFC candidate materials, coatings, processing, and test methodology. This is a goal the US Department of Energy has set forth in the Solid-State Energy Conversion Alliance's (SECA) Core Technology Program. The objective is to bridge the technology gap between research findings from small button cells and the full-sized stacks of industrial developers. The choice of planar over other designs was based on progress in anode-supported cell design with thin electrolyte (e.g., 10 microns or less) such that the typical operation temperature can be reduced from ~1000 °C to ~800 °C or less. At these temperatures the use of low-cost ferritic stainless steel with protective coatings appears feasible, although the long-term durability remains to be validated. The cell was a commercial NiO–YSZ anode-supported YSZ electrolyte with LSM cathode of nominal size 5 cm × 5 cm. Other shapes of cell in planar SOFC designs such as circular have also been demonstrated. For example, 1 kW class stacks with 50 circular anode-supported cells of 12 cm diameter were demonstrated to have an efficiency reaching 54% [23]. From a strength point of view, a circular shape would be preferred over square or rectangular shapes since corners can lead to high stress concentration. However, the circular shape tends to result in more waste in cell and interconnect plate fabrication, as well as longer machining time, and therefore was not adopted in this work. The current square cell size is smaller than the actual cells used by industrial developers, which are often in the range of 10–20 cm per side length, yet it still offers a reasonable area for studying new materials, etc., without requiring heavy investment in either test facilities (such as furnace, fuel, gas flow equipment, and electronic equipment) or the cells and stacks to be tested. We have also selected a cross-flow pattern for gases such that one of the gases was flowing in S–N direction while the other flowed in E–W direction. This flow arrangement allowed the separation of the internal manifolding into four quadrants and reduced the sealing constraints in small areas. Furthermore, 3-D modeling of thermal and gas flow distribution using computational fluid dynamics simulation code (STAR-CD version 3.05) predicted, in the present design, minimal temperature gradient and very small pressure drop (~5%) across each cell as well as between the three cells [24].

3.2. Long-term electrochemical performance

The electrochemical performance in terms of cell voltage versus time at 800 °C is shown in Fig. 3 for each cell. The cells were tested in constant current mode with a total current of 5 A (313 mA cm^{-2}). In Fig. 3, it is evident the top cell (see Fig. 2 for the cell configuration) showed the most stable behavior with minimum overall degradation. The bottom cell showed a distinct and much longer (~140 h) "activation" or "burn-in" process before stabilizing for about 1000 h, as compared to the top and middle cells where the activation process was minimal and rapid. There are many papers discussing the possible mechanisms behind the frequently observed improvement in cell performance during the initial stage of testing, which attribute the activation process to changes in surface chemistry, changes in bulk structure, and/or a combination of both. For example, Jiang et al. reported that the activation was due to reincorporation of SrO into the structure upon the cathodic polarization [25,26]. On the other hand, la O' et al. showed a surface enrichment of Sr and Mn upon cathodic polarization [27]. Based on a study of a thin LSM (600 nm) film deposited on YSZ electrolyte, McIntosh proposed two activation mechanisms in LSM cathodes: short-duration activation resulting from changes in surface chemistry, and long-duration activation resulting from reconstruction of the LSM phase [28]. A recent article has given extensive reviews of factors governing oxygen reduction mechanisms in cathodes [29]. In contrast to the bottom cell, both the middle and top cells showed very minute and rapid (~0.5 h) activation behavior (see inset in Fig. 3), consistent with the literature [25,26] and our previous study of the same anode-supported cell with LSM–YSZ cathode [12]. The cause for the longer activation behavior of the bottom cell, as compared to the other cells, was not clear but may be attributed to the structure changes as reported in literature [30–32]. Unfortunately, this could not be verified in the current long-term stability test since the total test duration of about 6000 h (after the initial ~140 h of activation process) could have overshadowed the morphological/structure changes in the early stage. Nonetheless, a comprehensive microstructure and interfacial characterization and analysis will be presented in part II and III of this work.

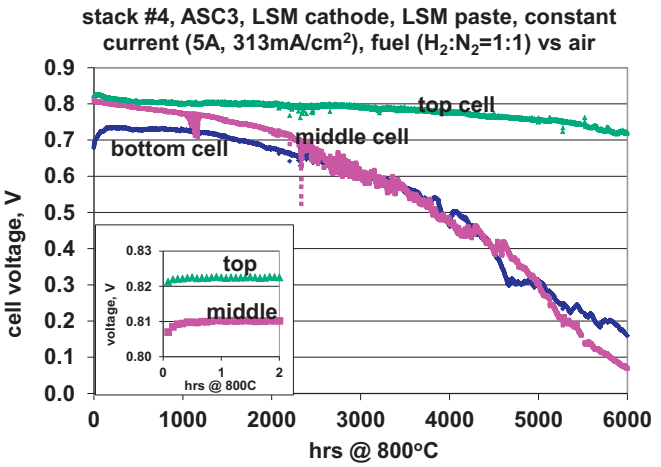

Fig. 3. Stability test of a 3-cell short stack in constant current mode (313 mA cm^2) at 800 °C. The fuel was H_2 in N_2 (1:1) with ~3% H_2O versus air. The inset shows the minimal and short "activation" behavior of the top and middle cells.

Regarding cell performance, the bottom cell started to degrade after around ~1300 h and showed more degradation and erratic behavior after about 2300 h. The middle cell appeared to degrade from the very beginning, and the degradation increased overtime with more erratic behavior afterward. The degradation rate of each cell in the first 1000 h, in terms of voltage change, was about 2.6% kh^{-1}, 4.5% kh^{-1}, and −6.9% kh^{-1} for the top, middle, and bottom cell, respectively. The bottom cell showed an improvement in cell performance, due to the distinct activation process when the cell voltage increased from the initial value of 0.674 V (0 h) to 0.732 V (140 h). For the second thousand hours of operation, the top

cell showed almost no degradation among the three cells with a degradation rate of 0.05% kh^{-1}, while the degradation rate was 6.4% kh^{-1} and 7.1% kh^{-1} for the middle and bottom cell, respectively. Afterward, the degradation appeared to increase with time and for the final ~1000 h (from t = 5000 h–6000 h) the degradation rate was 4.5%, 77%, and 50% kh^{-1} for the top, middle, and bottom cell, respectively. Such a high degradation rate as compared to the initial 2000 h data suggested some drastic extrinsic changes rather than intrinsic slow diffusion-dominated process such as reduction in gas transport from densification of active anode and/or cathodes, diminished triple phase boundaries due to grain growth, and oxide scale growth of metallic interconnect. Open circuit voltage measurements of each cell (Fig. 4) indicated that major leaks developed during the long-term test of the middle and bottom cells, for which the OCV clearly deviated from the initial values: 1.084 V (top cell), 1.063 V (middle cell), and 1.080 V (bottom cell). The middle cell's lower OCV was likely due to the current design in that the middle cell was more prone to leaks around the internal manifolding (referring to Figs. 1 and 2, the middle cell is facing two full interconnect plates with four slots for gas passage while the top and bottom cells only faced one such interconnect plate). The theoretical (Nernst) OCV would be about 1.064–1.051 V for the air and fuel (H_2:N_2 = 1:1 with ~3–5% H_2O) pair at 800 °C, assuming a 0.5% leakage of air into fuel (the 0.5% leakage was estimated based on typical leak rate of hybrid mica seals with Ag interlayers of 0.02–0.04 sccm per cm of leak length or total perimeter length). The initial OCVs of the three cells were all consistent with the Nernst values, suggesting no major leaks such as cell-to-frame failure or cell fracture. The middle cell's OCV started deviating from the Nernst value after 2000 h running, while the OCV of the other two cells remained fairly constant. The bottom cell also started to show a decrease in OCV after about 3500 h, and the quickly followed the same trend as the middle cell. Only the top cell remained constant during the entire 6000 h running. Note that there was about 10–20 mV fluctuation for the OCVs which can be attributed to temperature changes in the water bath used for fuel humidification.

Since the measured cell voltage is directly related to the OCV, one can differentiate or subtract the leakage-caused contribution to the measured cell voltage to estimate the "intrinsic" degradation of the cells. The final OCV (at 6000 h) was 1.068 V (top cell), 0.541 V (middle cell), and 0.591 V (bottom cell). The drop from initial OCVs

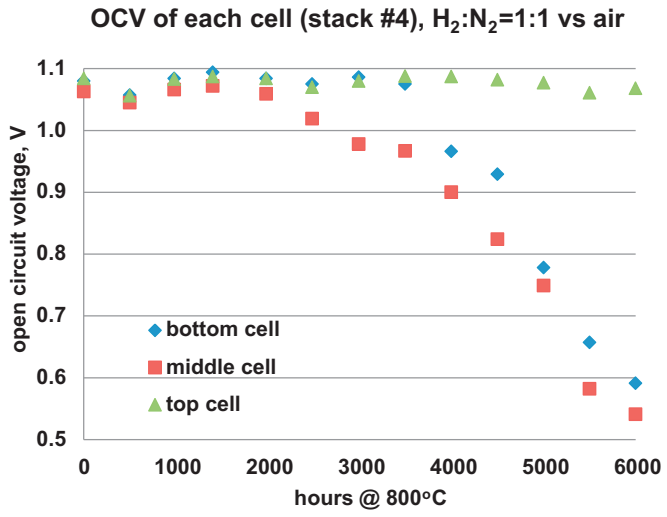

Fig. 4. OCV of individual cells during the long-term electrochemical stability test of a 3-cell short stack in constant current mode at 800 °C.

was 0.016 V (top cell), 0.522 V (middle cell), and 0.489 V (bottom cell). The measured cell voltage at the beginning of current discharge was 0.822 V (top cell), 0.810 V (middle cell), and 0.723 V (bottom cell, taken data at 140 h where the activation process appeared complete). The cell voltage at 6000 h was 0.722 V (top cell), 0.069 V (middle cell), and 0.160 V (bottom cell). Adjusted for the OCV drop one can calculate the average degradation for the entire period to be 1.70% kh^{-1} (top cell), 4.50% kh^{-1} (middle cell), and 1.74% kh^{-1} (bottom cell). The cell's adjusted degradation behavior of the top and bottom cells appeared very consistent with each other, while the middle cell was much less stable. There are limited publications regarding the long-term stability of Ni/YSZ supported YSZ electrolyte cell with LSM cathode in the stack geometry. Malzbender et al. recently reported a detailed microstructural analysis of a 19,000 h test on a 4 cell short stack at 800 °C using moist hydrogen (~3% H_2O) and air. The cell was 10 cm × 10 cm with a double-layer LSM ($La_{0.65}Sr_{0.3}MnO_3$). All the four cells showed similar degradation of about 5 mV kh^{-1} (about 0.6% kh^{-1}) until about 14,000 h at which time one of the cells showed a sudden loss of performance [33] and lower OCV than the other three cells. From detailed microstructural analysis they attributed the observed degradation to the diffusion of Mn from the LSM cathode into the 8YSZ electrolyte, which created electronic pathways for partial short-circuiting through the electrolyte. A short duration (<1000 h) test of a 3-cell short stack of similar materials and cell size at 750 °C in constant current mode followed by intermittent thermal cycling was also reported. During constant current operation, the stack showed no degradation in the initial ~200 h at 400 mA cm^{-2}, but the stack voltage decreased at higher current density of 600 mA cm^{-2} for the following 250 h. They attributed the drop of stack voltage to an increase in stack ASR from 0.667 Ω cm^{-2} to 0.731 Ω cm^{-2} which corresponded to a high degradation rate of ~38% kh^{-1} [34]. A larger sized (50 cm^2) single cell stack with LSM cathode was also tested for long-term (5500 h) stability at 750 °C. The results showed a clear dependence of performance loss on current densities ranging from 560 to 480 mA cm^{-2}, with a degradation rate of ~20% kh^{-1} [35]. When current density was reduced to 360 mA cm^{-2}, a reactivation was observed with performance improvement of ~2% kh^{-1} but this was followed by degradation of 5% kh^{-1} that accelerated to 10% kh^{-1} until the end of the test. The initial large degradation was suspected to be related to reoxidation of nickel anode at too high anode overpotential due to a limited supply of fuel [35]. The performance results in the present study (i.e., adjusted degradation rates of ~1.7% kh^{-1} for top and bottom cells) appeared to be consistent with Malzbender et al.'s data, although one must realize that direct comparison of stack performance is very difficult due to differences in processing and microstructure, fuel and air utilization, stack design, and seal system.

3.3. Post-mortem observation and failure analysis

After the 6000 h test, the short stack was dis-assembled from the test fixture for post-mortem analysis using optical microscopy. For each cell, there were two pairs of matching fracture surfaces to examine, one at the anode side and one at the cathode side, as shown in Figs. 5 and 6, respectively, for the top cell. Fig. 5 shows the fracture surface of the anode side of the cell (Fig. 5A) and the matching fracture surface of the Ni mesh of the interconnect plate (Fig. 5B). The matching fracture surfaces of the cathode side are shown in Fig. 6A (cathode) and Fig. 6B (interconnect plate). The cell appeared to be well bonded to the aluminized window frame plate in that no discoloration was found on the cell or along the sealing edges (dotted arrow in Fig. 5A). The cell's anode exhibited the typical gray color of the reduced state, indicative of a good seal.

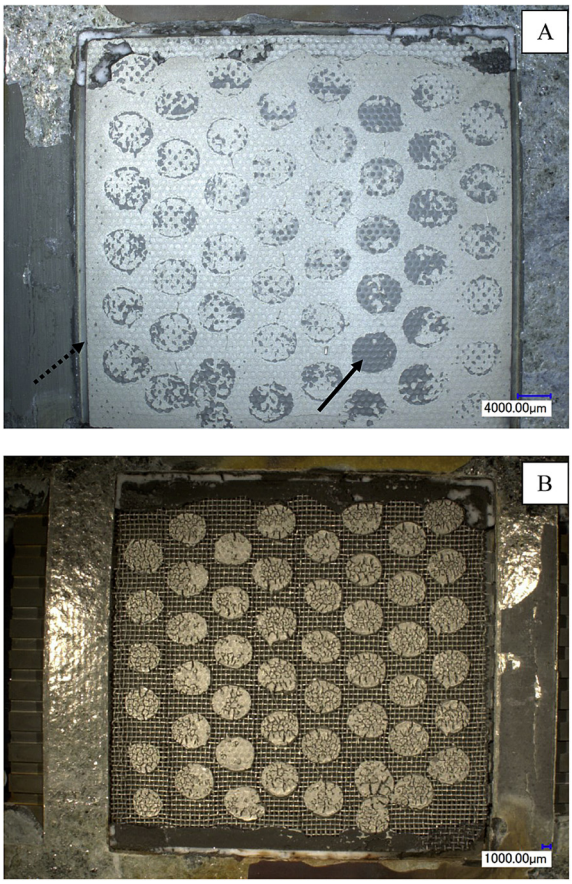

Fig. 5. Matching fracture surfaces of the anode side of top cell after long-term stability test of a 3-cell short stack. (A) Anode side of cell showing the Ni contacts, and (B) anode side of AISI441 interconnect plate showing the Ni mesh and contacts. The dotted arrow in (A) shows the sealing edges; the solid arrow shows the desired full contact where the thin Ni current collector layer was peeled off completely.

A closer look at the 49 contact spots revealed that the current contact processing was not optimized, as only a few spots showed the desired full contact (solid arrow in Fig. 5B) in which the Ni contact material (a few mm thick) embedded into the Ni mesh completely peeled off the thin (less than 10 microns) Ni current collector layer on top of the anode support, revealing the darker Ni–YSZ support underneath that layer. On the cathode side, the fracture occurred between the LSM contact material and the cathode surface, as shown in Fig 6, in that the LSM contact material appeared less well bonded to the cathode surface (Fig. 6A inside the dotted regions) than to the Ce-(Mn,Co)-spinel coated AISI441 interconnect plate (arrows in Fig. 6B). This was consistent with the fact that the spinel coating applied by ultrasonic spraying had a rougher surface than the screen printed cathode, which provided mechanical interlocking at the coating/LSM interface. In addition, there would be very limited solid state sintering between the LSM contact and LSM cathode at the current sealing temperature (950 °C) as compared to the typical sintering temperature (~1200 °C). Post-mortem images of the middle cell are shown in Fig. 7. Contrary to the top cell, the middle cell was completely peeled off from the window frame plate (Fig. 7A) and appeared strongly bonded on the anode side to the interconnect plate, revealing the black cathode side (Fig. 7B). Closer examination along the glass seal edges showed yellowish color (arrows in Fig. 7A and B), indicative of the formation of undesirable $SrCrO_4$, which has a very high CTE that can lead to failure of the glass seal upon thermal cycling. Similar yellowish color was also observed for the bottom cell; this was attributed to a poor quality alumina coating along the window frame edges. An earlier study of joint strength of refractory sealing glass with Crofer22APU showed that the strength was completely degraded by the formation of $SrCrO_4$ [21]. In addition to the chromate formation, dimensional changes and related stress redistribution (as discussed in the next section) can also assist the glass seal failure. Overall, the glass seal failure was consistent with the observed OCV drop during the long-term test, which led to the accelerated degradation in electrical performance of the middle and bottom cells.

3.4. Issue of dimensional control for stack test

For planar type SOFCs, a compressive loading or some type of clamping mechanism is often required to hold the multiple tens of repeating cells and interconnect plates together; otherwise the cells and interconnect plates may lose contact due to different warping behavior between mating parts from temperature gradients. The temperature gradient in our current 3-cell stack is small, but it can be large for the full-sized stacks. The typical operating temperature for planar SOFCs is around 800 °C, which is higher than the softening point of most glass-ceramic type of sealing glasses before crystallization [14], as well as the less crystallizable compliant glasses [36]. At these elevated temperatures and under compressive stresses, in addition to creep of metallic interconnects and mica seals, the glass seal can deform or show viscous flow. The nominal compressive loading for the current stack test, 0.2 MPa (30 psi), was considered to be evenly distributed across the 5 cm × 5 cm cell, frame, and

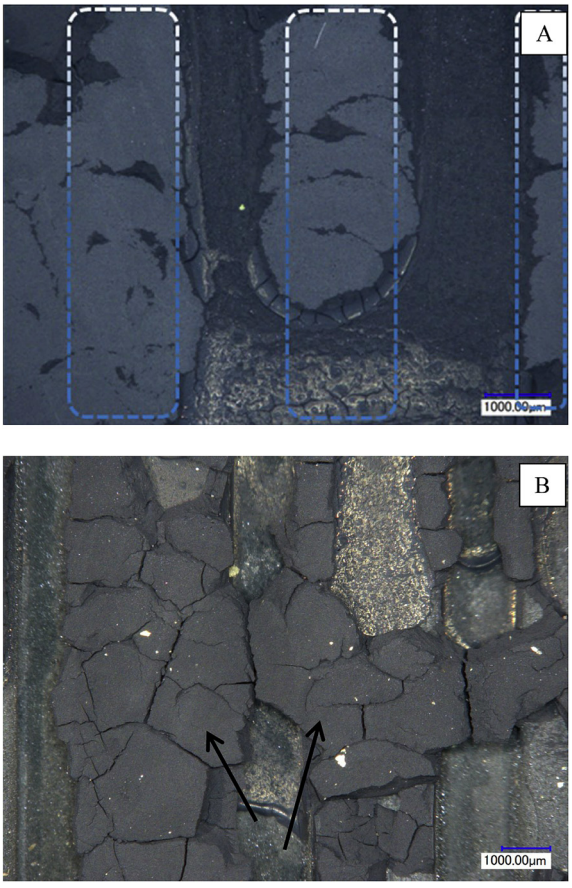

Fig. 6. Matching fracture surfaces of the cathode side of top cell after long-term stability test of a 3-cell short stack. (A) Cathode side of PEN cell with dotted lines showing the LSM contact regions, and (B) cathode side of Ce-(Mn,Co) spinel coated AISI441 interconnect plate showing the LSM contacts (arrows).

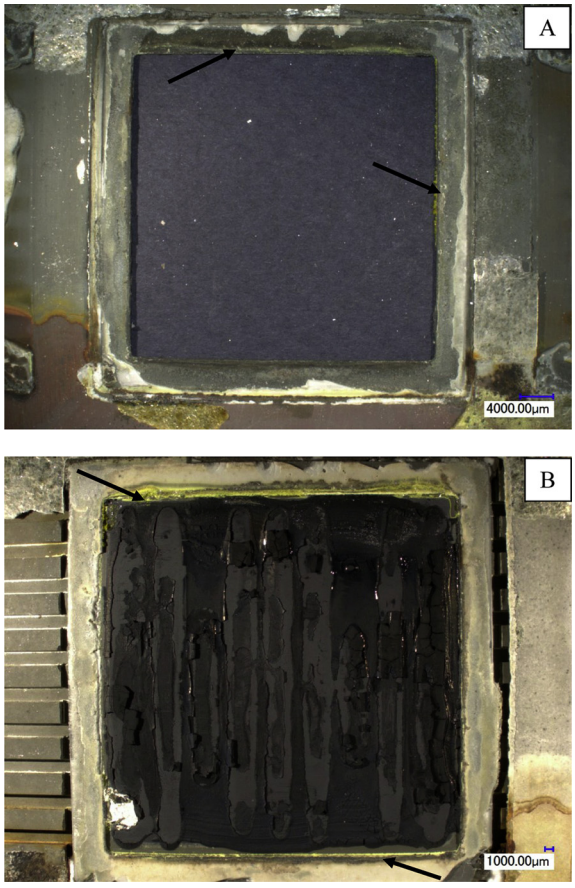

Fig. 7. Post-mortem analysis of the middle cell, (A) the window frame plate where the cell was peeled off, (B) peeled off middle cell bonded to interconnect plate showing the cathode side. Note the yellowish color (arrows) along the perimeter of the black cathode indicates the formation of $SrCrO_4$ which led to the glass seal failure. (For interpretation of the references to color in this figure legend, the reader is referred to the web version of this article.)

interconnect plates before anode reduction. After the anode has been fully reduced along with the Ni contact paste and Ni mesh, one can assume that the compressive stresses would redistribute since the cathode side with the LSM contact material would be relatively rigid compared to the soft and compliant Ni contact and mesh. As a result, a tensile stress will occur along the glass seal (as shown by red arrows in Fig. 8), leading to glass seal failure. In addition, the hybrid mica (mica sandwiched between two glass layers) and the perimeter metal parts (AISI441) could also creep under the compressive loading. However, the contribution from metal creep would likely be insignificant as compared to that from the hybrid micas. The hybrid mica for the perimeter seal was composed of a phlogopite mica sandwiched by glass layers about 250 microns thick on either side. The glass (G18) was shown to easily creep under nanoindentation even at 400 °C [37]. The compressive creep of AISI441 is not known but compressive creep is often an order of magnitude smaller than tensile creep. The tensile creep of a similar material (Crofer22APU) was investigated at 25–800 °C [38] and the published data suggested the creep rupture life at 800 °C would be over 10^6 h at applied stress of 1 MPa; the creep behavior would be much less at 0.2 MPa.

4. Summary and conclusion

A "generic" stack test fixture was developed at Pacific Northwest National Laboratory to enable the assessment of SOFC candidate materials and processing methods under realistic conditions. A three-cell short stack was assembled and tested with the generic fixture at 800 °C for 6000 h to evaluate the long-term behavior of candidate materials (refractory sealing glass, alumina and (Mn,Co)-spinel coating, ferritic stainless steel AISI441, and hybrid mica perimeter seal) using a commercial anode-supported thin YSZ electrolyte cell with an LSM-based cathode. In part one, the test fixture design, seal system, and interconnect plates were addressed. Cell electrochemical performance showed a low degradation rate of ~1.4% kh^{-1} for top cell where no glass seal failure was observed. For the middle and bottom cells rapid degradation was observed and was correlated to open circuit voltage. Post-mortem analysis showed characteristic yellowish $SrCrO_4$ formation, indicating glass seal failure. The causes of the glass seal failure were addressed and attributed to incomplete alumina coating as well as inadequate dimensional control. Overall, the current generic stack fixture serves as a viable and economic tool to assess SOFC candidate materials and processing to bridge the gap between laboratory scale button cells and full-sized stacks.

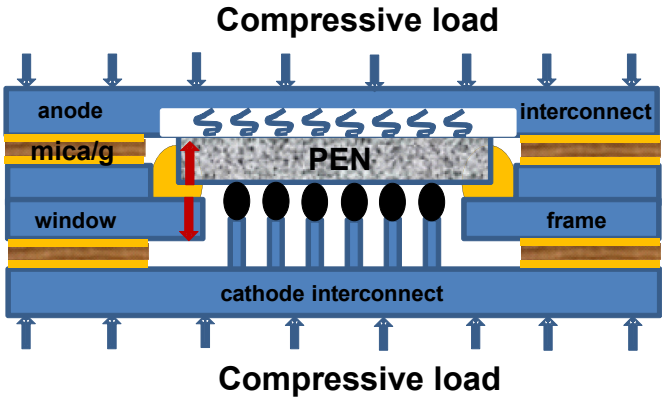

Fig. 8. Schematic showing the cross-section view of a complete cell with anode interconnect plate, and cathode interconnect plate. Note that stress redistribution could induce a tensile stress (red arrows) on glass seal (yellow) after anode reduction and the creep of mica and the metal parts. (For interpretation of the references to color in this figure legend, the reader is referred to the web version of this article.)

Acknowledgment

The authors would like to thank S. Carlson for SEM sample preparation, and J. Coleman for SEM analysis. This work summarized in this paper was funded by the US Department of Energy's Solid-State Energy Conversion Alliance (SECA) Core Technology Program. The authors would like to thank Briggs White and Shailesh Vora from NETL for helpful discussions. Pacific Northwest National Laboratory is operated by Battelle Memorial Institute for the US Department of Energy under Contract no. DE-AC06-76RLO 1830.

References

[1] S.P. Simner, M.D. Anderson, G.-G. Xia, Z. Yang, L.R. Pederson, J.W. Stevenson, J. Electrochem. Soc. 152 (4) (2005) A740–A745.
[2] P. Kim, D.J.L. Brett, N.P. Brandon, J. Power Sources 189 (2) (2009) 1060–1065.
[3] B. Liu, Y. Zhang, B. Tu, Y. Dong, M. Cheng, J. Power Sources 165 (1) (2007) 114–119.
[4] J. Mermelstein, M. Millan, N. Brandon, J. Power Sources 195 (6) (2010) 1657–1666.
[5] W. Wang, M.D. Gross, J.M. Vohs, R.J. Gorte, J. Electrochem. Soc. 154 (5) (2007) B439–B445.
[6] H. Yokokawa, T. Horita, N. Sakai, K. Yamaji, M.E. Brito, Y.-P. Xiong, H. Kishimoto, Solid State Ionics 177 (7) (2006) 3193–3198.

[7] S. Taniguchi, M. Kadowaki, H. Kawamura, T. Yasuo, Y. Akiyama, Y. Miyake, T. Saitoh, J. Power Sources 55 (1) (1995) 73–79.
[8] Y.D. Zhen, A.I. Tok, S.P. Jiang, F.Y.C. Boey, J. Power Sources 170 (1) (2007) 61–66.
[9] K. Fujita, K. Ogasawara, Y. Matsuzaki, T. Sakurai, J. Power Sources 131 (2) (2004) 261–269.
[10] T. Komatsu, R. Chiba, H. Arai, K. Sato, J. Power Sources 176 (1) (2008) 132–137.
[11] W.N. Liu, X. Sun, E. Stephens, M.A. Khaleel, J. Power Sources 189 (2) (2009) 1044–1050.
[12] Y.-S. Chou, J.W. Stevenson, J.-P. Choi, Int. J. Appl. Ceram. Technol. 8 (1) (2011) 23–32.
[13] Y.-S. Chou, J.W. Stevenson, J.-P. Choi, Int. J. Appl. Ceram. Technol. 9 (2) (2012) 1–10.
[14] Y.-S. Chou, J.W. Stevenson, P. Singh, J. Electrochem. Soc. 154 (7) (2007) B644–B651.
[15] K.D. Meinhardt, D.-S. Kim, Y.-S. Chou, K.S. Weil, J. Power Sources 182 (1) (2008) 188–196.
[16] Y.-S. Chou, J.W. Stevenson, J. Power Sources 191 (2) (2009) 384–389.
[17] Y.-S. Chou, J.W. Stevenson, J. Power Sources 140 (2) (2005) 340–345.
[18] Z. Yang, G.-G. Xia, C.-M. Wang, Z. Nie, J. Templeton, J.W. Stevenson, P. Singh, J. Power Sources 183 (2) (2008) 660–667.
[19] Z. Yang, G. Xia, Z. Nie, J. Templeton, J.W. Stevenson, Electrochem. Solid-State Lett. 11 (8) (2008) B140–B143.
[20] Z. Yang, K.D. Meinhardt, J.W. Stevenson, J. Electrochem. Soc. 150 (8) (2003) A1095–A1101.
[21] Y.-S. Chou, J.W. Stevenson, P. Singh, J. Power Sources 185 (2) (2008) 1001–1008.
[22] J.-P. Choi, K. Scott Weil, Y.-S. Chou, J.W. Stevenson, Z.-G. Yang, Int. J. Hydrogen Energy 36 (7) (2011) 4549–4556.
[23] M. Yokoo, Y. Tabata, Y. Yoshida, H. Orui, K. Hayashi, Y. Nozaki, K. Nozawa, H. Arai, J. Power Sources 184 (1) (2008) 84–89.
[24] K.P. Recknagle, unpublished work.
[25] S.P. Jiang, L.G. Love, J.P. Zhang, M. Hoang, Y. Ramprakash, A.E. Hughes, S.P.S. Badwal, Solid State Ionics 121 (1–4) (1999) 1–10.
[26] W. Wang, S.P. Jiang, Solid State Ionics 177 (15–16) (2006) 1361–1369.
[27] G.J. la O', R.F. Savinell, Y. Shao-Horn, J. Electrochem. Soc. 156 (6) (2009) B771–B781.
[28] M.A. Haider, S. McIntosh, J. Electrochem. Soc. 156 (12) (2009) B1369–B1375.
[29] S.B. Alder, Chem. Rev. 104 (10) (2004) 4791–4843.
[30] S.P. Jiang, J.G. Love, Solid State Ionics 158 (1–2) (2003) 45–53.
[31] M. Kuzneecov, P. Otschik, P. Obenaus, K. Eichler, W. Schaffrath, Solid State Ionics 157 (1–4) (2003) 372–378.
[32] Y. Huang, J.M. Vohs, R.J. Gorte, J. Electrochem. Soc. 152 (7) (2005) A1347–A1353.
[33] J. Malzbender, P. Batfalsky, R. Vaben, V. Shemet, F. Tietz, J. Power Sources 201 (3) (2012) 196–203.
[34] H.Y. Jung, S.-H. Choi, H. Kim, J.-W. Son, J. Kim, H.-W. Lee, J.-H. Lee, J. Power Sources 159 (1) (2006) 478–483.
[35] M. Molinelli, D. Larrain, N. Autissier, R. Ihringer, J. Sfeir, N. Badel, O. Bucheli, J. Van herle, J. Power Sources 154 (3) (2006) 394–403.
[36] Y.-S. Chou, E.C. Thomsen, R.T. Williams, J.-P. Choi, N.L. Canfield, J.F. Bonnett, J.W. Stevenson, A. Shyam, E. Lara-Curzio, J. Power Sources 196 (5) (2011) 2709–2716.
[37] J. Milhans, M. Khaleel, X. Sun, M. Tehrani, M. Al-Haik, H. Garmestani, J. Power Sources 195 (5) (2010) 3631–3635.
[38] Y.-T. Chiu, C.-K. Lin, J.-C. Wu, J. Power Sources 196 (4) (2011) 2005–2012.